Chapter 9

Laser-Produced Heavy Ion Plasmas as Efficient Soft X-Ray Sources

Takeshi Higashiguchi, Padraig Dunne and Gerry O'Sullivan

Additional information is available at the end of the chapter

http://dx.doi.org/10.5772/63455

Abstract

We demonstrate extreme ultraviolet (EUV) and soft x-ray sources in the 2- to 7 -nm spectral region related to the beyond extreme ultraviolet (BEUV) question at 6.*x* nm and a water window source based on laser-produced high-Z plasmas. Strong emissions from multiply charged ions merge to produce intense unresolved transition array (UTA) toward extending below the carbon K-edge (4.37 nm). An outline of a microscope design for single-shot live- cell imaging is proposed based on a high-*Z* UTA plasma source, coupled to x-ray optics. We will discuss the progress and Z-scaling of UTA emission spectra to achieve lab-scale table-top, efficient, high-brightness high-Z plasma EUV-soft x-ray sources for *in vivo* bio-imaging applications.

Keywords: High-*Z*, unresolved transition array (UTA), extreme ultraviolet (EUV), soft x-ray, water window

1. Introduction

Laboratory- scale source development of shorter- wavelength spectral regions in the extreme ultraviolet (EUV) and soft x-ray has been motivated by their applications in a number of high-profile areas of science and technology. One such topic is the challenge of three-dimensional imaging and single-shot flash photography of microscopic biological structures, such as macromolecules and cells, *in vivo*. For x-ray microscopy, the x-ray source should emit a sufficient photon flux to expose the image of the biosample on the detector. Recently, the most practical source of high-power, high-brightness x-rays has been radiation from synchrotrons and x-ray– free electron lasers (XFEL) [1]. Compact sources using liquid nitrogen droplets are being developed for the use of the zone plates for the transmission microscopy. Recently, the wavelength at 2.48- nm narrowband emission from a liquid-nitrogen-jet laser-plasma [2] was

successfully combined with the latest normal-incidence multilayer condenser optics and 20-nm zone-plate optics to work laboratory water-window x-ray microscopy [3] with resolution less than 25 nm and synchrotron-like image quality on biological and environment science samples. The development of a high-brightness source based on a focused electron beam impacting a liquid water jet resulting in 2.36-nm emission has also been studied [4]. The total collected energy, however, is low, when one combines the narrowband line emission with the low reflection coefficient of the collector mirror. As a result, long exposures are needed to take a picture, and there is not yet published evidence of single-shot, flash exposures by the use of a laboratory-scale source. In order to overcome the low efficiency imposed by line emission sources, we propose the use of high- power water-window emission from laser-produced high-Z plasmas, analogous to the extending scheme of efficient, high-volume manufacturing EUV sources.

High-power EUV sources with high efficiency for semiconductor lithography at 13.5 [5] and 6.7 nm [6–8] based on laser-produced plasmas (LPP) have been demonstrated in high-volume manufacturing of integrated circuits (IC) having node sizes of 22 nm or less [9, 10]. The EUV emission at the relevant wavelength may be coupled with La/B_4C or Mo/B_4C multilayer mirror with a reflectivity of 40% to provide a source at 6.5–6.7 nm. Recently, a reflection coefficient of about 60–70% was shown to be feasible in a theoretical study [11]. Consequently, the development of a new wavelength EUV source for the next- generation semiconductor lithography, which can be coupled with an efficient B_4C multilayer mirror, is particularly timely.

High-Z element plasmas of Sn and Gd produce strong resonant band emission due to 4d–4f and 4p–4d transitions around 13.5 nm and 6.7 nm, respectively, which are overlapped in adjacent ion stages to yield the intense unresolved transition arrays (UTAs) in their spectra. The in-band high-energy emissions are attributable to hundreds of thousands of near-degenerate resonance lines lying within a narrow wavelength range. Rare earth elements gadolinium (Gd) and terbium (Tb) produce strong resonant emission in an intense UTA around 6.5–6.7 nm [6–8]. The choice of these elements was prompted by the use of UTA radiation in tin (Sn) for the strong 13.5-nm emission, where $n = 4–n = 4$ transitions in Sn ions overlap to yield an intense UTA [12, 13], as the optimum source for 13.5 nm and the scaling of this emission to the shorter wavelength with increasing Z. Because the emitting ions in Gd and Tb plasmas have largely a similar electronic structure to Sn, they are expected to have a similar spectral behavior and emit an intense UTA due to 4d–4f and 4p–4d transitions at shorter wavelengths.

Plasmas of the rare earth elements gadolinium (Gd) and terbium (Tb) produce strong resonant emission due to the presence of an intense UTA around 6.5–6.7 nm in the spectra of their ions [6]. In tin (Sn), the presence of the corresponding feature at 13.5 nm prompted its selection as the optimum source material at that wavelength. The UTA emission scales to shorter wavelength with increasing atomic number, Z. Because the emitting ions in Gd ($Z = 64$) and Tb ($Z = 65$) plasmas have an electronic structure largely similar to Sn, they are expected to exhibit a similar spectral behavior and emit an intense UTA due to 4d–4f and 4p–4d transitions at shorter wavelengths. Recently, the suitability of Nd:yttrium-aluminum-garnet (Nd:YAG) LPP EUV sources based on Gd and Tb has been demonstrated for high- power operation [6]. Since at

http://dx.doi.org/10.5772/63455

high plasma electron densities, the opacity effects reduce the intensity of the resonance lines thereby limiting the output power, methods of reducing the effects of reabsorption (opacity) were evaluated to achieve high energy conversion efficiency (CE) from the incident laser energy to the EUV emission energy and the spectral purity. The effect of optical thickness was evaluated by changing the laser wavelength to alter the plasma electron density [7, 14]. In order to increase the EUV energy CE and spectral efficiency (purity), the optical thickness in the dominant region of the EUV emission of high-*Z* highly charged plasmas should be controlled. To enhance the EUV emission from Gd plasmas, it is important to reduce reabsorption by the resonance lines and the emission from satellite lines that attribute to the long wavelength side of the array around 6.7 nm to improve the spectral purity as well as increase the resonance emission intensity [7]. In order to achieve this, we used low initial –density targets for the Nd:YAG LPPs [8]. In low-density, optically thin plasmas, a suppression of the reabsorption effect and the satellite emission, which originates from the high electron and ion density region, is expected, similar to the results obtained with low-density Sn targets used to optimize the emission from the Nd:YAG LPP EUV sources at 13.5 nm [15, 16]. It is known that optically thick plasmas can strongly self-absorb resonance emission. Optically, thin plasmas provide more efficient sources. Therefore, systematic LPP UTA source studies with up-to-date intense picosecond pulse lasers [17] or middle infrared laser, such as the CO_2 laser [14], are needed to determine available light source wavelengths for future applications.

In this chapter, we show the efficient EUV and soft x-ray sources in the 2- to 7- nm spectral region related to the beyond extreme ultraviolet (BEUV) question at 6.*x* nm and a water window source based on laser-produced high-*Z* plasmas. Resonance emission from multiply charged ions merges to produce intense UTA spectral structure, extending below the carbon K-edge (4.37 nm). An outline of a microscope design for single-shot live cell imaging is proposed based on a high-*Z* plasma UTA source, coupled to x-ray optics. We discuss the progress and *Z*-scaling of UTA emission spectra to achieve lab-scale table-top, efficient, high-brightness high-*Z* plasma EUV–soft x-ray sources for *in vivo* bioimaging applications.

2. Characteristics of the Gd plasmas for BEUV source applications

In order to increase the energy CE from the incident laser energy to the interested wavelength emission energy with the defined bandwidth, it is important to suppress not only the reabsorption by assurance of the plasma is optically thin but also plasma hydrodynamic expansion loss, while maintaining a plasma electron temperature of T_e = 100−120 eV [6, 17]. Lateral expansion of the plasma causes kinetic energy losses, which reduce the energy available for radiation and is particularly important for small focal spot diameters [6]. For practical EUV source development, it is important to establish the optimum plasma condition related to laser irradiation condition and construct a database of properties of the UTA plasma EUV sources. In addition, to compare with one-dimensional (1D) numerical simulation, it is important to produce 1D expansion plasmas by irradiating multiple laser beams based on the laser inertial confinement fusion (ICF) geometry [18]. Laboratory- scale experiments have, to date, only been studied under 2D conditions due to the use of a single laser beam and small focal spot

diameters. Under multiple laser irradiation, it is expected that the highest CE will be achieved as plasma expansion loss can be neglected in plasmas from targets irradiated by solid-state laser pulses. In the database point of view, we demonstrate high CE for the EUV emission around 6.7 nm from multiple laser beam –produced 1D spherical plasmas of rare earth elements of Gd and Tb. The maximum in-band EUV CE at 6.7 nm within a 0.6% bandwidth (0.6%BW) in a solid angle of 2π sr was observed to be 0.8%, which is twice as large as that obtained by the use of a Joule-class laboratory- scale single laser beam with 2D or 3D plasma expansion losses. The CE value was one of the highest ever reported due to the reduction of the plasma expansion loss applying 12 laser beams under 1D plasma expansion condition.

A Nd:glass laser system, GEKKO-XII at the Institute of Laser Engineering (ILE) in Osaka University was used to produce the 1D expanding uniform plasma [19]. The GEKKO-XII laser facility consists of 12 laser beams each at a wavelength of 1.053 μm and a constant 1 J pulse energy, irradiating a total energy of 12 J, with a temporal Gaussian- shaped pulse width of 1.3 ns [full width at half maximum (FWHM)]. The 12 laser beams were located at 12 faces of a regular dodecahedron to irradiate spherical targets uniformly. A thick metallic layer of 2 μm was coated onto spherical polystyrene balls for providing targets. The laser power imbalance was monitored to be within ± 6.3% of the average. Then, the laser beams were uniformly irradiated onto the target, to provide a 1D plasma expansion with low expansion loss.

Figure 1 shows the temporal history of the in-band emission around 6.7 nm with the bandwidth of 0.6% from Gd plasmas observed by the x-ray streak camera to provide 1D time-resolved imaging. The red and blue lines are the EUV emission at the optimum intensity of 1×10^{12} W/cm^2 and the maximum intensity of 3×10^{13} W/cm^2, respectively. Under optimum irradiation conditions with the highest CE, the temporal profile of the EUV emission was similar of that of the laser pulse shown by the dashed line and reached a maximum a little later. On the other hand, the behavior of the EUV emission profile at 3×10^{13} W/cm^2 initially rose faster, but the peak was delayed by comparison with that obtained under optimum conditions. The initial steep rise indicates that the electron temperature quickly reaches a value necessary for the in-band EUV emission. The final electron temperature is expected to be higher than optimum, so that higher charge state ions higher than q = 28 are produced, which predominantly emit shorter- wavelength out-of-band emission around 2–4 nm. After the maximum electron temperature is attained, plasma recombination proceeds accompanied by adiabatic expansion, resulting in cooling. The in-band emission from ionic charge states of $q \approx 20$ arises in the recombination phase. Then, the time- resolved emission consists of a fast rising component and a delayed peak relative to the laser pulse. This measurement suggests that the temporal shape of the in-band emission should essentially behave similarly to the laser pulse shape under optimum laser irradiation conditions.

The in-band EUV CEs were evaluated at $\lambda = 6.7$ nm within a bandwidth of 0.6% for Gd and Mo and at $\lambda = 6.5$ nm with the bandwidth of 0.6% for Tb. The CEs were maximized at 0.8% in both Gd and Tb at $I_L = 1 \times 10^{12}$ W/cm^2, and the observed maximum CE was almost in agreement with the theoretical evaluation of 0.9% obtained from a collisional–radiative (CR) and modified 1D hydrodynamic code numerical simulation [21]. It is noted that the wavelength of 6.6 nm, predicted in the work, is slightly different compared to our spectral peaks at 6.5 and 6.7 nm.

http://dx.doi.org/10.5772/63455

A decrease in CE was also observed at the laser intensity higher than 1×10^{12} W/cm^2. Around these intensities, the rare earth highly charged plasmas are overheated, the average ionization stage increases and the population of relevant ions with $q \approx 20$ decreases. Then, the CE decreases due to the increase in electron temperature [20].

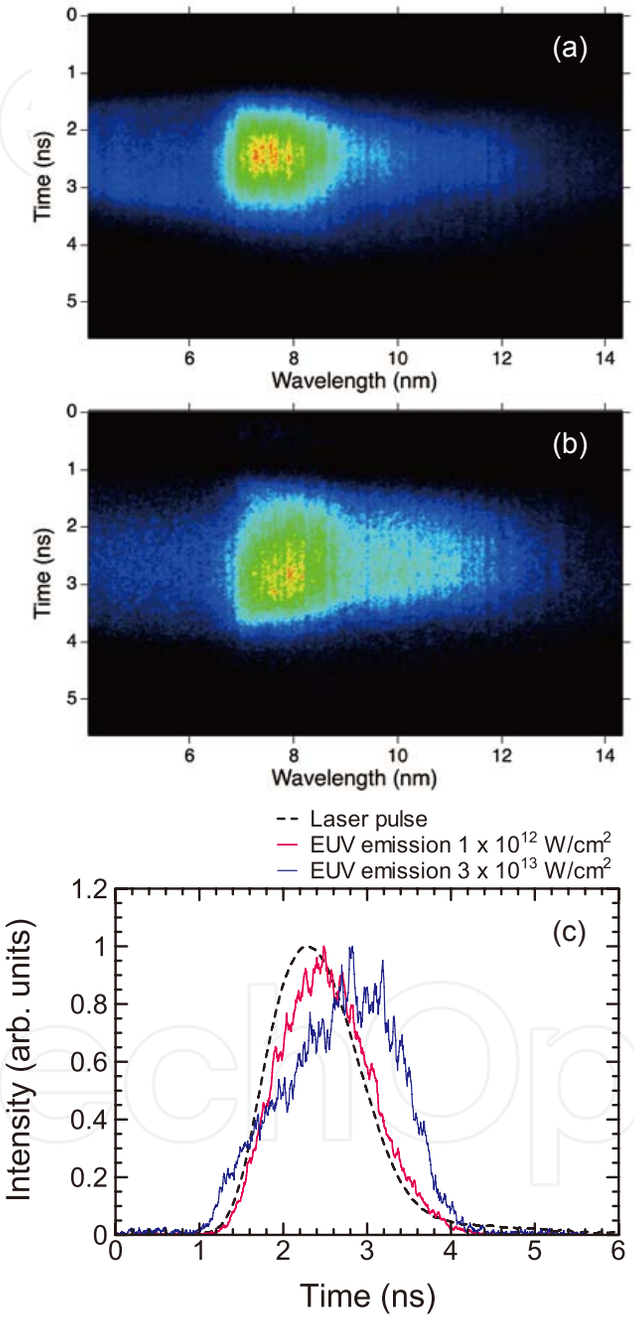

Figure 1. Time-resolved spectral images at two different laser intensities of (a) 1×10^{12} W/cm^2 and (b) 3×10^{13} W/cm^2, respectively. (c) Temporal histories of the EUV emission at 6.7 nm from Gd plasmas at two different laser intensities of 1×10^{12} W/cm^2 (red) and 3×10^{13} W/cm^2 (blue), together with a temporal profile of the laser pulse (dashed). At an optimum laser intensity of 1×10^{12} W/cm^2, the temporal behavior of the in-band emission is essentially the same as that of the laser pulse. It should be noted that intensities are normalized for timing comparison [20].

In addition, it is important to understand the physics of the EUV emission and transport in laser-produced dense high-Z plasmas. In order to achieve an efficient light source, or to diagnose complex highly charged ion (HCI) plasmas, the evaluation of plasma parameters is of fundamental importance in order to benchmark radiation hydrodynamic simulation codes. One matter of fundamental physics is the relationship between the electron density profile and the dominant EUV emission region. In general, dense high-Z plasmas are optically thick in the EUV spectral region, and the EUV emission originates from regions of reduced electron density where there is not only sufficient emissivity but also lower effects from opacity. We describe the results of measurements of the electron density profile of a laser produced isotropically expanding spherical Gd plasma using a Mach-Zehnder interferometer, as shown in Figure 2 [22]. The interferometry was performed at a wavelength of 532 nm to enable penetration of the plasmas to a high -density region, which has a maximum density close to the critical density of 1×10^{21} cm^{-3} as set by the plasma initiating laser wavelength of 1.053 μm. The EUV emission was observed using a monochromatic EUV pinhole camera. We present benchmark data for the electron density profile with the dominant EUV emission at 6.7 nm occurring in a region with an electron density close to 10^{19} cm^{-3} [14], which was corresponded to the critical density of the CO_2 (carbon dioxide) laser LPP, as shown in Figure 3 [22].

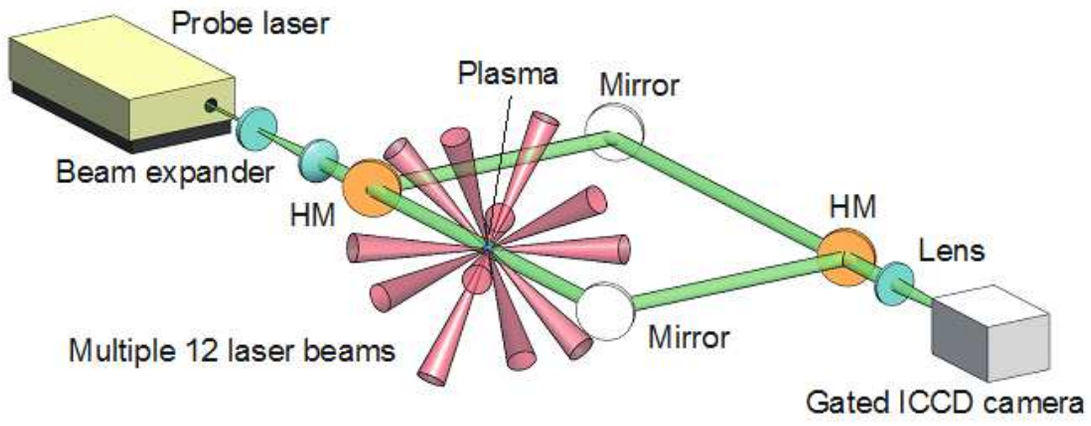

Figure 2. Schematic diagram of the experimental setup. Interferograms were produced by a Mach-Zehnder interferometer by the use of a Nd:YAG laser at a wavelength of 532 nm with a pulse duration of 6 ns (FWHM) [22].

The production of low-density plasma by the use of CO_2 LPPs has been proposed, because the critical electron density n_{ec} depends on the laser wavelength, λ_L, i.e., $n_{ec} \propto \lambda_L^{-2}$. The critical density at a laser wavelength of $\lambda_L = 10.6$ μm for a CO_2 laser is two orders of magnitude smaller than at $\lambda_L = 1.06$ μm for the solid-state laser. Then, a suppression of reabsorption and satellite emission in the wavelength region longer than 6.x nm is expected in CO_2 LPPs due to the lower plasma electron density. By extending efficient CO_2 laser–produced Sn plasma EUV sources around 13.5 nm, the CE and spectral efficiency, which is important when considering out-of-band spectral suppression, should be increased in an optically thin plasma. In order to ascertain the applicability of a CO_2 LPP EUV source at 6.x nm, its behavior needs to be clarified in a manner similar to the work performed on CO_2 LPP EUV sources at 13.5 nm.

http://dx.doi.org/10.5772/63455

We characterize the EUV emission from CO_2 laser–produced plasmas (CO_2-LPPs) of the rare earth element of Gd. The energy CE and the spectral purity in the CO_2-LPPs were higher than that for solid-state LPPs at 1.06 μm, because the plasma produced is optically thin due to the lower critical density, resulting in a maximum CE of 0.7% at 6.76 nm with 0.6% bandwidth in the solid angle of 2π sr. The peak wavelength was fixed at 6.76 nm for all laser intensities. The plasma parameters at a CO_2 laser intensity of 1.3×10^{11} W/cm^2 was also evaluated using the hydrodynamic simulation code to produce the EUV emission at 6.76 nm.

Figure 4(a) shows time-integrated EUV emission spectra from the Nd:YAG-LPPs at different laser intensities ranging from 9.7×10^{11} to 6.6×10^{12} W/cm^2. The peak wavelength shifts from 6.7 to 6.8 nm and is mainly due to $n = 4–n = 4$ ($\Delta n = 0$) transitions in HCIs with an open 4*f* or 4*d* outermost subshell. The sharp peak at 6.65 nm and the dip structure below 6.59 nm first appear at a laser intensity of 2.4×10^{11} W/cm^2. The emission at wavelengths less than 6 nm, increases with increasing laser intensity, and according to numerical evaluation, lines in the λ = 2.5–6 nm ($h\nu$ = 207–496 eV) spectral region originate from Gd ionic charge states between Gd^{19+} and Gd^{27+} and arise from $n = 4–n = 5$ ($\Delta n = 1$) transitions [14].

In the case of CO_2-LPPs, the main spectral behaviors near 6.7 nm, on the other hand, are narrower than for Nd:YAG laser irradiating plasma, as shown in Figure 4(b). The CO_2 laser intensity was varied from 5.5×10^{10} to 1.2×10^{11} W/cm^2. The spectral structure was dramatically different to that from the Nd:YAG-LPPs. The peak wavelength of 6.76 nm remains constant with the increase of the laser intensity. Moreover, the emission intensity of the peak at 6.76 nm increases more rapidly with laser intensity than the emission in the ranges of λ = 3–6.6 nm and λ = 6.8–12 nm, respectively. Under the optically thin plasma conditions imposed by the CO_2-LPPs, this peak, which is mainly due to the $4d^{10}\ {}^1S_0–4d^9 4f\ {}^1P_1$ transition of Pd-like Gd^{18+} overlapped with $^2F–^2D$ lines of Ag-like Gd^{17+}, known to lie around 6.76 nm shows that these ions are indeed present in the plasma. Similar structure has been also observed in a discharge-produced plasma, which has low density and is optically thin like the CO_2-LPP. It is noted that

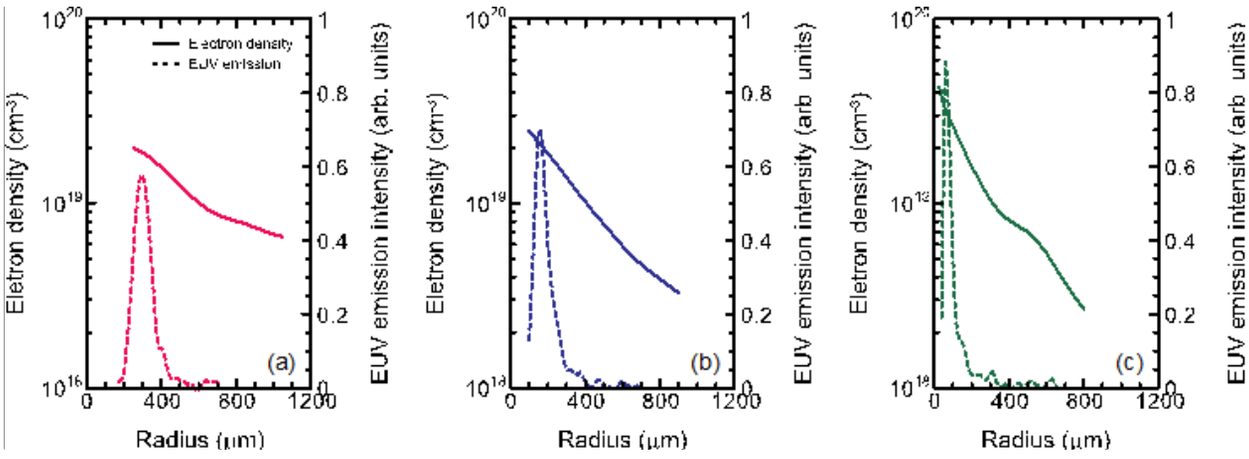

Figure 3. Profiles of the radial electron density (solid line) and radial EUV emission (dashed line) at the time of three different peak laser intensities of (a) 1×10^{12} W/cm^2, (b) 7×10^{12} W/cm^2, and (c) 1×10^{14} W/cm^2, corresponding to laser focal spot and target diameters of (a) 500 μm, (b) 200 μm, and (c) 50 μm [22].

the peak wavelength of 6.76 nm was constant with high spectral efficiency (purity) and energy CE in optically thin CO_2-LPPs of Gd [14].

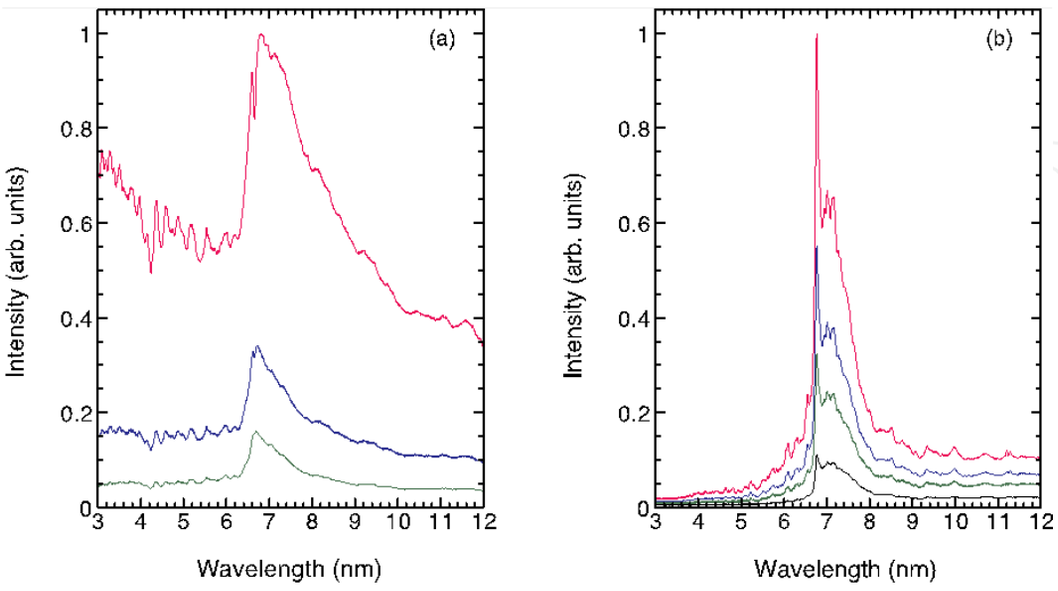

Figure 4. (a) Time-integrated EUV emission spectra from the Nd:YAG LPPs at different laser intensities of 9.7×10^{11}, 2.2×10^{12}, and 6.6×10^{12} W/cm^2, respectively. The peak wavelength shifts from 6.7 to 6.8 nm with increasing the laser intensity. (b) Time-integrated EUV emission spectra from the CO_2 LPPs at different laser intensities of 5.5×10^{10}, 8×10^{10}, 9.8×10^{10}, and 1.3×10^{11} W/cm^2, respectively. The peak wavelength of 6.76 nm remains constant with increasing the laser intensity [14].

In order to infer the laser parameters that maximize 6.*x*-nm Gd-LPP emission, direct comparison between emissions from a laser-produced Gd plasma and that of Gd ions from well-defined charge states is necessary, as the charge state dependence of the emission at 6.*x* nm is defined by the electron temperature. We present a study of the charge state–defined emission spectra to explain the laser power density dependence of the Gd-LPP spectra and to evaluate the charge states contributing to the 6.*x*-nm emission.

The profile of the intense emission at 6.*x* nm becomes broader, and its peak wavelength shifts to longer wavelength with increasing laser power density, as shown in Figure 5(a). However, the range of wavelengths involved is quite small, and the peak lies between 6.7 and 6.8 nm over this entire range of power densities. The emission from each of these peak wavelengths within a 0.6%BW becomes more intense with increasing laser flux. This behavior causes difficulty in fixing the precise wavelength of 6.*x* nm and optimization of the spectral efficiency while simultaneously maximizing the CE. The spectral efficiency denotes the ratio of the in-band energy at 6.70 nm within a 0.6%BW to that in the spectral ranging from 3 nm to 12 nm. An increase in laser power density raises the electron temperature which, in turn, implies an increase of both the highest charge state and the abundance of higher charge states. This change in the ion population must cause the observed shift of the peak wavelength for Gd-LPPs. Up to now, there was no direct experimental evidence that changes in emitting ion populations were responsible for this shift.

http://dx.doi.org/10.5772/63455

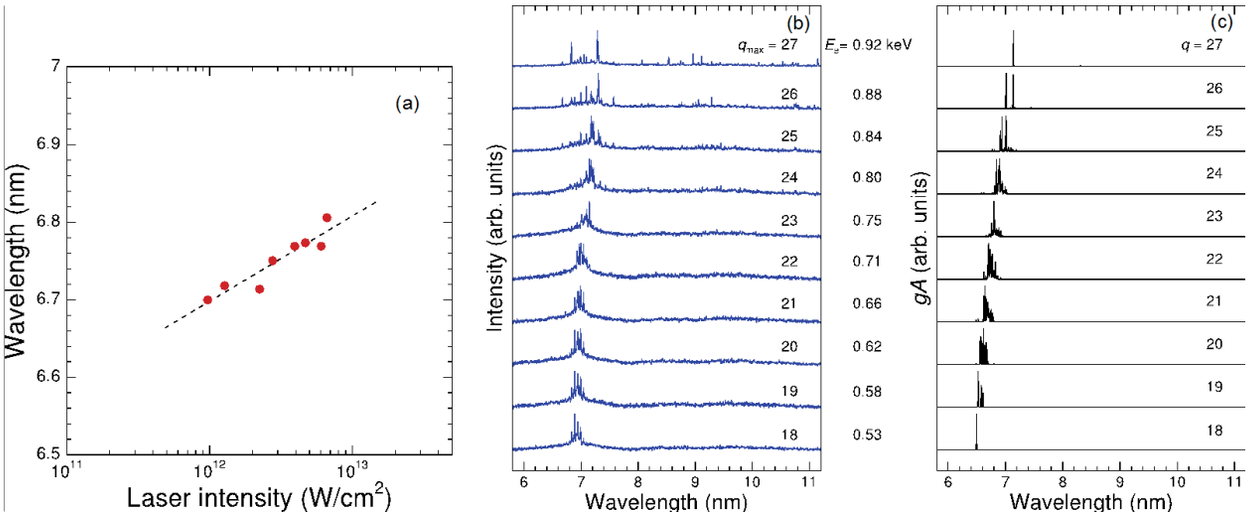

Figure 5. (a) The wavelength of the emission peaks near 6.*x* nm as a function of the Nd:YAG laser power density. The dotted line is a fitted curve. (b) EUV emission spectra of Gd ions with electron beam energies (E_e) of 0.43–0.92 keV. In the case of E_e = 0.43 keV, the compact EBIT with lower resolution was employed, while the Tokyo-EBIT was used in other cases. (c) Calculated *gA* values for 4*d*–4*f* transitions of the corresponding highest charge states (q_{max}) from Figure 5(b). The ground configuration of Gd^{18+} is [Kr]$4d^{10}$ [23]. Note that *q* is the charge state of Gd in Figures 5(b) and 5(c).

To verify the above explanation, charge-defined emission spectra were measured with the EBITs for different highest charge states. EUV emission spectra from EBIT experiments are shown in Figure 5(b), and calculated *gA* values of 4*d*–4*f* transitions for corresponding highest charge states are shown in Figure 5(c) to compare the charge state dependence of the emission near 6.*x* nm. The *gA* values are the transition probabilities from excited states multiplied by their statistical weights and thus are proportional to the emission intensities of the transitions. Note that the EBIT spectra include a subset of all possible radiative transitions that are predominantly resonant transitions to the ground state. For Pd-like Gd^{18+}, only one strong line is predicted corresponding to the $4d^{10}\ {}^1S_0$–$4d^9 4f\ {}^1P_1$ at 6.7636 nm, and this is clearly seen in the spectrum. In the absence of the configuration interaction (CI), according to the UTA model, the position of the intensity-weighted peak of the $4d^N$–$4d^{N-1}4f$ array depends directly on the occupancy of the 4*d* subshell, *N*, and the Slater-Condon $F^k(4d,4f)$ and $G^k(4d,4f)$ parameters. In the present case, the values of F^k and G^k change little with ionization stage, and therefore, the position of the array moves to lower energy with decreasing *N*. The presence of CI causes this shift to be reduced, but nevertheless, the overall trend is to move to longer wavelength with increasing ionization stage. The dominant emissions around 7 nm in the EBIT spectra indeed move to longer wavelengths with an increase of the highest charge state. The EBIT can thus generate charge- defined emission spectra, which are essential for both analysis of plasma emission spectra and the benchmarking of theoretical calculations [23].

3. Quasi-Moseley's law for the UTA emission

In this section, we show that the strong resonance UTAs of Nd:YAG LPPs for elements with *Z* = 50–83 obey a quasi-Moseley's law [24]. A 150-ps Nd:YAG laser with a maximum energy

of 250 mJ at λ_L = 1.064 μm and an 8-ns Nd:YAG laser giving 400 mJ at λ_L = 1.064 μm were employed to provide the desired variation of laser intensity. The laser beam was incident normally onto planar high-Z metal targets in vacuo. The expected focal spot size, produced by an anti–reflection- coated plano-convex BK7 lens with a focal length of 10 cm, had a FWHM of approximately 50 μm. The laser was operated in single shot mode, and the target surface was translated to provide a fresh surface after each laser shot. A flat-field grazing incidence spectrometer (GIS) with an unequally ruled 2400 grooves/mm grating was placed at 30° with respect to the axis of the incident laser. Time-integrated spectra were recorded by a Peltier-cooled back-illuminated charge-coupled device (CCD) camera and were corrected by its quantum efficiency. The typical resolution was better than 0.005 nm (FWHM). The Large Helical Device (LHD) is one of the largest devices for magnetically confined fusion research and is described in detail elsewhere. The LHD plasmas were produced by the injection of a small amount of target elements into the background hydrogen plasma. The plasma density is about 10^{13} cm^{-3}, much lower than that in a LPP, and guarantees an optically thin condition. Emission spectra were recorded by a 2-m grazing incidence Schwob-Fraenkel spectrometer with a 600 grooves/mm grating. The exposure time of the detector was set at 0.2 s, and the spectral resolution is about 0.01 nm (FWHM).

Figures 6(a) −6(k) show LPP emission spectra from high-Z metal targets. The main UTA peak at 8.17 nm in the case of Nd clearly shifts to shorter wavelength with increasing atomic number, 3.95 nm in the case of Bi. This movement indicates the availability of a wide wavelength range for a LPP light source. While the main UTA peaks correspond to $4p^6 4d^N – 4p^6 4d^{N-1} 4f$ transitions, the $4p^6 4d^N – 4p^5 4d^{N+1}$ UTAs were also observed around them, at 4 nm for the LPP of Pt, in the case of 150-ps LPPs. Optically thinner LHD plasma spectra are shown in Figures 6(l) −6(q). It should be noted that the electron temperatures of LHD plasma were relatively low, ≤ 1 keV, but higher than in 150-ps LPPs [24].

As a result, we have not observed significant emission of the type $4f^N – 4f^{N-1} 5l$ from stages with open 4f valence subshells in LHD spectra. Comparing LPP and LHD spectra, the UTA widths in LHD spectra are relatively narrower than in LPPs especially for lighter elements. This arises as a result of a number of factors: the increased contributions from ions with an outermost $4d^{10} 4f^N$ configuration from transitions of the type $4d^{10} 4f^N – 4d^9 4f^{N+1}$ in LPP spectra and the differences in opacity that reduce the intensity of the strongest lines and the increased contribution from satellite emission. In addition, earlier research demonstrated that if the majority of radiation originates from open 4f subshell ions, whose complexity inhibits the emission of strong isolated lines, then no strong isolated lines are expected to appear throughout the EUV emission, which is clearly seen for the LPP spectra in Figure 6. Moreover, self-absorption effects are clearly observed in the case of 10-ns LPP for Nd due to optical thickness. Although the n = 4–n = 4 UTA transition peak was observed at 8.05 nm in the LHD spectrum, the strongest 4d–4f transitions essentially disappear in the 10-ns LPP owing to self-absorption. Because of their large transition probabilities, resonant lines that are strong in emission also strongly absorb in underdense ($n_e < n_{ec}$) or optically thick plasma conditions. An optically thinner plasma reduces the self-absorption effects and increases the spectral efficiency of n = 4–n = 4 UTA emissions.

http://dx.doi.org/10.5772/63455

Figure 7 shows the atomic number dependence of the observed peak wavelength of $n = 4–n = 4$ UTAs. The solid line is an approximated curve for 150-ps LPPs with a power-law scaling of the peak wavelength given by $\lambda = aR_0^{-1}(Z - s)^{-b}$ in nm, where $a = 21.86 \pm 12.09$, $b = 1.52 \pm 0.12$, $s = 23.23 \pm 2.87$ is the screening constant while Slater's rule gives $s = 36–39.15$ for $4d$ electrons, and R_0 is the Rydberg constant. This empirical law is surprisingly similar to Moseley's law, where $a = 4/3$, $b = 2$, and $s = 1$ were used to give the transition wavelength of the $K\alpha$-line of characteristic x-rays. It is noted that the Moseley's law derived from the Bohr model gives $\lambda = 0$ for $\Delta n = 0$ transitions in terms of the energy difference. It can, however, be fitted as a quasi-Moseley's law because there are energy differences between $\Delta n = 0$ levels due to different angular momentum quantum numbers [24].

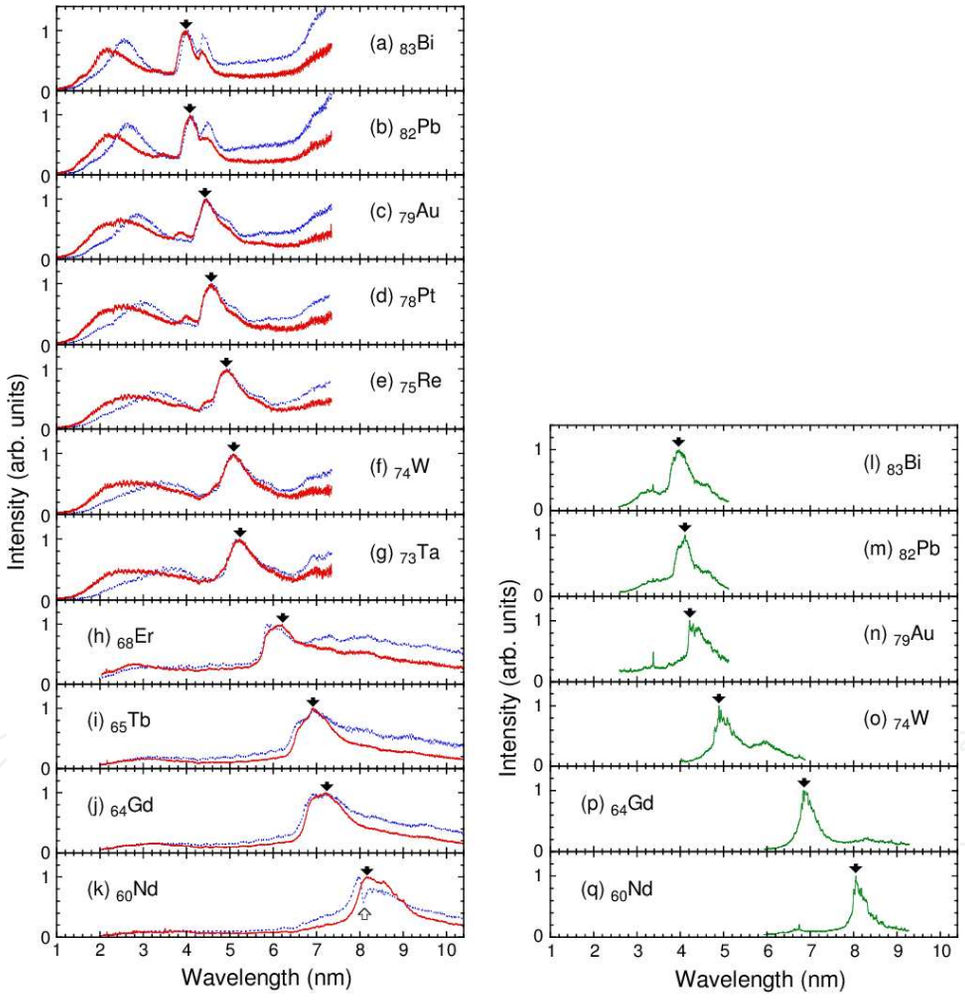

Figure 6. Time-integrated EUV emission spectra of the Nd:YAG LPPs for (a) $_{83}$Bi, (b) $_{82}$Pb, (c) $_{79}$Au, (d) $_{78}$Pt, (e) $_{75}$Re, (f) $_{74}$W, (g) $_{73}$Ta, (h) $_{68}$Er, (i) $_{65}$Tb, (j) $_{6}$4Gd, and (k) $_{6}$0Nd targets with 150-ps laser (red, solid line) and 10-ns laser (blue, dotted line), respectively. Typical laser power densities were 2.5×10^{14} W/cm^2 for ps-laser illumination and 5.6×10^{12} W/cm^2 for 10-ns laser irradiation. The measured LHD spectra (green, solid) for (l) Bi, (m) Pb, (n) Au, (o) W, (p) Gd, and (q) Nd targets, respectively. An emission line at 3.4 nm is from impurity carbon ions. Intensities were normalized at each maximum of the $n = 4–n = 4$ UTAs. Solid arrows indicate peak position of $n = 4–n = 4$ UTAs of 150-ps LPP and LHD spectra. An open arrow indicates structure due to self-absorption [24].

We propose here a pathway to produce feasible laboratory-scale high-Z LPP sources for a wide range of applications. For efficient UTA emission, plasmas of higher-Z elements need high-electron temperatures to produce higher charge state ions contributing to the $4p^6 4d^N – 4p^6 4d^{N-1} 4f$ UTAs. The electron temperature, T_e, rises with increasing laser intensity, such as $T_e \propto (I_L \lambda_L^2)^{0.4}$, where I_L and λ_L are the laser intensity and wavelength, respectively [25]. On the other hand, an optically thin plasma has a low electron density, n_e, which decreases with increasing λ_L. In terms of these features, use of a longer laser wavelength is necessary to generate the brightest LPP, such as a CO_2 laser operating at 10.6 μm due to the low critical density of 1×10^{19} cm^{-3} attainable with a pulse duration sufficiently short to give a laser intensity of the order of 10^{13} W/cm^2 but sufficiently long to permit excitation to the appropriate ionization stages, i.e., ~ 1 ns. Moreover, we can also obtain longer wavelengths, > 10.6 μm, with a Raman conversion system.

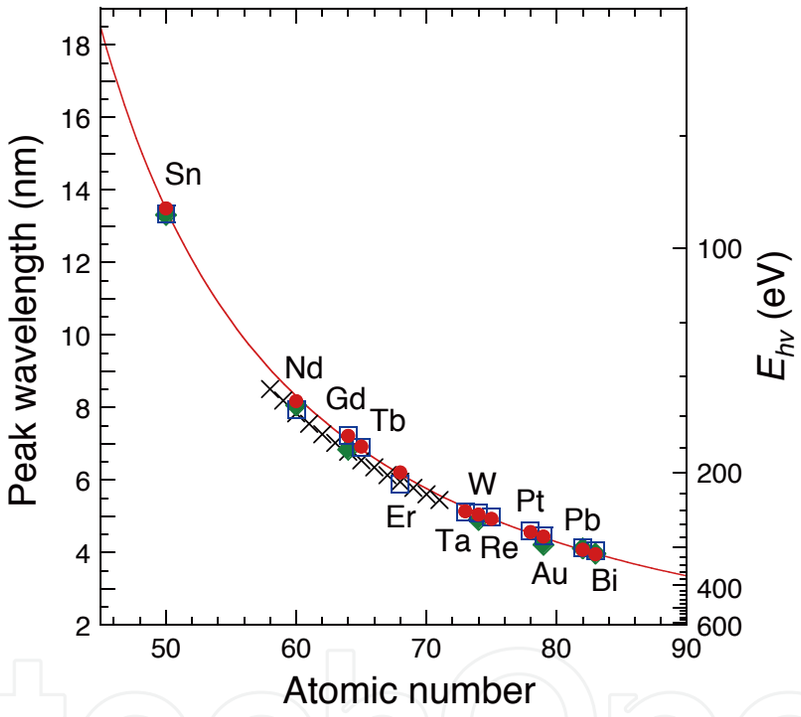

Figure 7. Atomic number dependence of the peak wavelength of $n = 4–n = 4$ UTAs in 150-ps LPP (red, circles), 10-ns LPP (blue, squares), and LHD (green, diamonds) spectra. Calculated peak wavelengths with GRASP are also shown (black, crosses). Sn spectra are not shown in Figure 6. The solid line is an approximated curve for $n = 4–n = 4$ UTAs in 150-ps LPPs with a power-law scaling [24].

4. Water window soft x-ray source by high-Z ions

4.1. Spectroscopy of low electron temperature in lab-scale laser-produced ions

According to the quasi-Moseley's law in Figure 7, the elements from $_{79}$Au to $_{83}$Bi are one of the candidates for high-flux UTA source in water window soft x-ray sources for single-shot (flash)

http://dx.doi.org/10.5772/63455

bio-imaging in the laboratory size microscope, because the UTA emission is essentially high-power emission due to much resonant lines around the specific wavelength (photon energy). The UTA peak wavelengths of $_{79}$Au, $_{82}$Pb, and $_{83}$Bi reach the water window soft x-ray spectral region.

Figures 8(a) −8(c) show time-integrated spectra from Au, Pb, and Bi plasmas at a laser intensity of the order of 10^{14} W/cm^2 with a pulse duration of 150 ps (FWHM). The time-integrated soft x-ray spectra between 1 and 6 nm from each element display strong broadband emission around 4 nm, which is mainly attributed to the n = 4–n = 4 transitions from HCIs with an open 4*f* or 4*d* outermost subshell with the broadband emission of 2–4 nm originating from the n = 4–n = 5 transitions from HCIs with an outermost 4*f* subshell. The intensity of the n = 4–n = 4 UTA emission was higher than that of the n = 4–n = 5 transition emission. The atomic number dependence of the spectral structure is shown in Figure 8(d). The predicted emission photon energy of each peak photon energy was shifted to higher photon energy with the increase of the atomic number. Neither the emission spectra nor the plasma electron temperatures, however, have been optimized, as shown below. However, the emission intensity of the n = 4–n = 5 transitions was compared with that of the n = 4–n = 4 transitions of the UTA emission [26].

We compared the results of numerical calculation for some different experimental temperatures with the observed spectra as shown in Figure 9(a). Four regions corresponding to emission peaks were identified. The emission in the region of "1" results primarily from the 4*f*–5*g* transitions in HCIs with an open 4f subshell, i.e., the stages lower than 35+ Bi ions. The emission in regions of "2" and "3" originates from 4*p*–4*d* and 4*d*–4*f* transitions with an open 4*d* subshells of Bi^{36+}–Bi^{45+}, and numerical calculations show that the higher- energy region results from the more highly ionized species higher than Bi^{42+}. The emission in the region of "4" was also associated mainly with the 4*d*–4*f* transition emission from lower ionic charge stages with an open 4*f* outmost subshell. As a result, the bulk of the emission, especially from regions of "1" and "4", was associated with the recombining phase of the expanding plasma plume. We evaluate for comparison spectra calculated for steady-state electron temperatures of 180 and 700 eV, while the higher temperatures were required to produce the emission in the region of "2", the calculations verify that both the longer and shorter wavelength features were consistent with much lower plasma electron temperatures [26].

In Figure 9(b), evaluated spectra at different electron temperatures higher than 900 eV were shown. Numerical calculations show that high-Z plasmas at an electron temperature lower than 700 eV, as shown in Figure 6(a), radiate strongly around 3.9 nm. In the case of higher electron temperatures from 800 to 1500 eV, the strongest emission, however, is expected at around 3.2 nm, suitable for coupling with Sc/Cr multilayer mirrors. Therefore, for an optimized source, we should produce a plasma at high electron temperature of around 1 keV. The emission intensity of the Bi plasma was compared with 2.48-nm nitrogen line emission from a Si_3N_4 planar target, in the same experimental setup, and was observed to be 1.2 times higher within a bandwidth of 0.008 nm (FWHM) even though the plasma electron temperature was much lower than the optimum value [26].

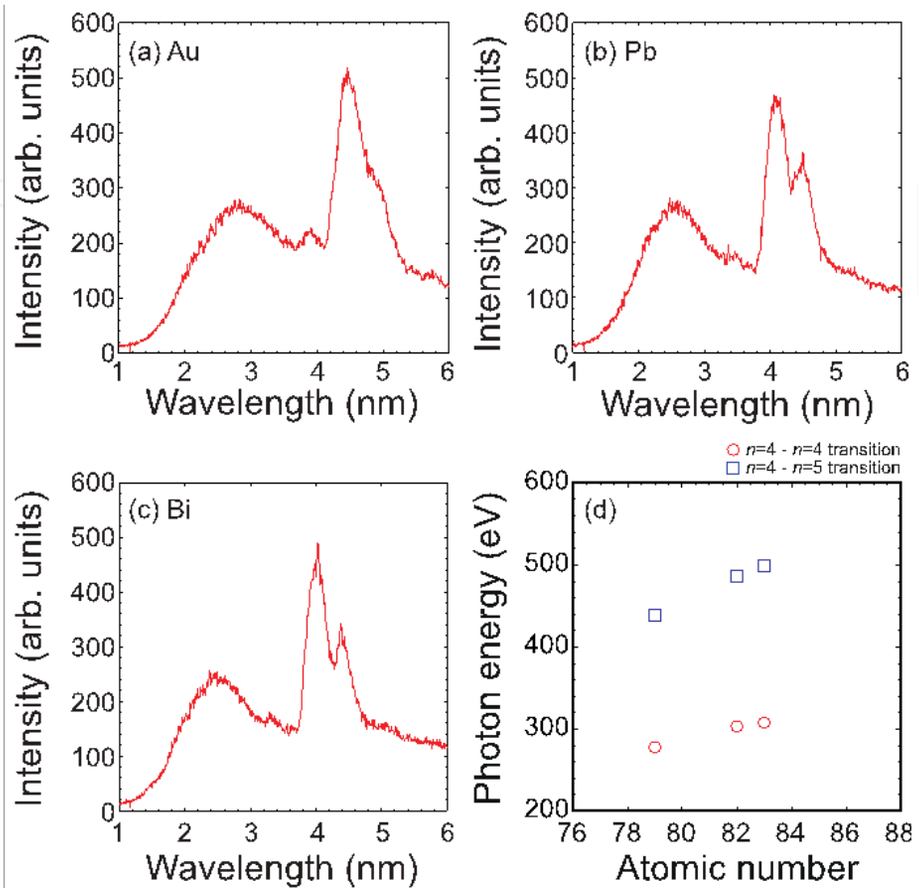

Figure 8. Time-integrated spectra from the picosecond-laser–produced high-*Z* plasmas by the use of Au (a), Pb (b), and Bi (c), and the atomic number dependence of the photon energies of the peak emission of the $n = 4$–$n = 4$ transition (circles) and the $n = 4$–$n = 5$ transition (rectangles) (d) [26].

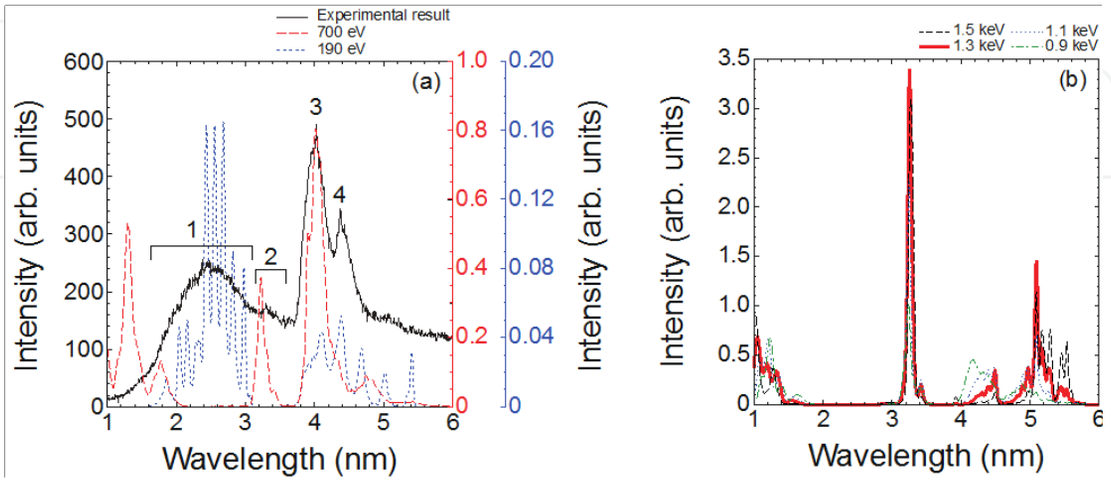

Figure 9. (a) The comparison between the observed spectrum with numerical calculation under assuming steady-state electron temperatures of 190 and 700 eV. (b) Calculated spectra for electron temperatures higher than 900 eV. [26]

4.2. Toward the laboratory water window soft x-ray microscope

Because of the broadband features of the emission, the zone plate components cannot be used, so one of the possible solutions would be to use a transmission planar x-ray nano-waveguide to image the sample. In order to achieve high resolution in the recorded image, we should also replace the recording device from the x-ray CCD camera to the sensitive EUV resist to overcome the resolution limitation of the CCD pixel size, coupling with the Schwarzschild optics, consisting of Sc/Cr multilayer mirrors. Although our proposal is based on a simple microscope construction, the key component is the UTA emitted from a hot dense Bi plasma point source, combined with Sc/Cr MLMs and sensitive EUV resists based on the photochemical reaction [26].

5. Summary

We have shown EUV and soft x-ray sources in the 2- to 7- nm spectral region related to the BEUV question at 6.*x* nm and a water window source based on laser-produced high-*Z* plasmas. The efficient 6.*x*-nm BEUV sources have been demonstrated at the CE of 0.7% due to the high spectral purity by the optically thin plasmas after the database experiments. According to the atomic number dependence of the UTA emission, so- called quasi-Moseley's law, the Bi HCI plasma source is one of the solutions in the laboratory single-shot (flash) bio-imaging by extending the UTA light source feature.

Author details

Takeshi Higashiguchi[1*], Padraig Dunne[2] and Gerry O'Sullivan[2]

*Address all correspondence to: higashi@cc.utsunomiya-u.ac.jp

1 Department of Electrical and Electronic Engineering, Faculty of Engineering, Utsunomiya University, Utsunomiya, Tochigi, Japan

2 School of Physics, University College Dublin, Belfield, Dublin, Ireland

References

[1] Gorniak T, Heine R, Mancuso A. P, Staier F, Christophis C, Pettitt M. E, Sakdinawat A, Treusch R, Guerassimova N, Feldhaus J, Gutt C, Grübel G, Eisebitt S, Beyer A, Gölzhäuser A, Weckert E, Grunze M, Vartanyants I. A, Rosenhahn A: X-ray holographic microscopy with zone plates applied to biological samples in the water win-

dow using 3rd harmonic radiation from the free-electron laser FLASH. Optics Express. 2011;19:11059–11070. DOI: 10.1364/OE.19.011059]

[2] Jansson P. A. C, Vogt U, Hertz H. M: Liquid nitrogen jet laser plasma source for compact soft x-ray microscopy. Review of Scientific Instruments. 2005;76:043503. DOI: 10.1063/1.1884186

[3] Takman P. A. C, Stollberg H, Johansson G. A, Holmberg A, Lindblom M, Hertz H. M: High-resolution compact X-ray microscopy. Journal of Microscopy. 2007;226:175–181. DOI: 10.1111/j.1365-2818.2007.01765.x

[4] Skoglund P, Lundström U, Vogt U, Hertz H. M: High-brightness water-window electron-impact liquid-jet microfocus source. Applied Physics Letters. 2010;96:084103. DOI: 10.1063/1.3310281

[5] Bakshi V, editor. EUV Sources for Lithography. Bellingham: SPIE Press Book; 2006. 1094 p. DOI: 10.1117/3.613774

[6] Otsuka T, Kilbane D, White J, Higashiguchi T, Yugami N, Yatagai T, Jiang W, Endo A, Dunne P, O'Sullivan G: Rare-earth plasma extreme ultraviolet sources at 6.5–6.7 nm. Applied Physics Letters. 2010;97:111503. DOI: 10.1063/1.3490704; and references therein.

[7] Otsuka T, Kilbane D, Higashiguchi T, Yugami N, Yatagai T, Jiang W, Endo A, Dunne P, O'Sullivan G: Systematic investigation of self-absorption and conversion efficiency of 6.7 nm extreme ultraviolet sources. Applied Physics Letters. 2010;97:231503. DOI: 10.1063/1.3526383

[8] Higashiguchi T, Otsuka T, Yugami N, Jiang W, Endo A, Li B, Kilbane D, Dunne P, O'Sullivan G: Extreme ultraviolet source at 6.7 nm based on a low-density plasma. Applied Physics Letters. 2011;99:191502. DOI: 10.1063/1.3660275

[9] Meiling H, Boeij W, Bornebroek F, Harned N, Jong I, Meijer H, Ockwell D, Peeters R, Setten E, Stoeldraijer J, Wagner C, Young S, Kool R, Kürz P, Lowisch M: From performance validation to volume introduction of ASML's NXE platform. Proceedings of SPIE. 2012;8322:83221G. DOI: 10.1117/12.916971

[10] Wagner C, Harned N: EUV lithography: Lithography gets extreme. Nature Photonics. 2010;4:24–26. DOI: 10.1038/nphoton.2009.251

[11] Platonov Y, Rodriguez J, Kries M, Louis E, Feigl T, Yulin S. Status of Multilayer Coatings for EUV Lithography. In: Proceedings of 2011 International Workshop on EUV Lithography; 13-17 June 2012; Maui (Hawaii). Austin: EUV Litho, Inc.; 2012. p. 49 (P25).

[12] O'Sullivan G, Carroll P. K: 4*d*–4*f* emission resonances in laser-produced plasmas. Journal of the Optical Society of America. 1981;71:227–230. DOI: 10.1364/JOSA.71.000227

[13] Carroll P. K, O'Sullivan G: Ground-state configurations of ionic species I through XVI for Z = 57–74 and the interpretation of 4*d*–4*f* emission resonances in laser-produced plasmas. Physical Review A. 1982;25:275–286. DOI: 10.1103/PhysRevA.25.275

[14] Higashiguchi T, Li B, Suzuki Y, Kawasaki M, Ohashi H, Torii S, Nakamura D, Takahashi A, Okada T, Jiang W, Miura T, Endo A, Dunne P, O'Sullivan G, Makimura T: Characteristics of extreme ultraviolet emission from mid-infrared laser-produced rare-earth Gd plasmas. Optics Express. 2013;21:31837–31845. DOI: 10.1364/OE.21.031837; and references therein.

[15] Okuno T, Fujioka S, Nishimura H, Tao Y, Nagai K, Gu Q, Ueda N, Ando T, Nishihara K, Norimatsu T, Miyanaga N, Izawa Y, Mima K: Low-density tin targets for efficient. Applied Physics Letters. 2006;88:161501. DOI: 10.1063/1.2195693

[16] Higashiguchi T, Dojyo N, Hamada M, Sasaki W, Kuobdera S: Low-debris, efficient laser-produced plasma extreme ultraviolet source by use of a regenerative liquid microjet target containing tin dioxide (SnO_2) nanoparticles. Applied Physics Letters. 2006;88:201503. DOI: 10.1063/1.2206131

[17] Cummins T, Otsuka T, Yugami N, Jiang W, Endo A, Li B, O'Gorman C, Dunne P, Sokell E, O'Sullivan G, Higashiguchi T: Optimizing conversion efficiency and reducing ion energy in a laser-produced Gd plasma. Applied Physics Letters. 2012;100:061118. DOI: 10.1063/1.3684242

[18] Yamanaka C, Kato Y, Izawa Y, Yoshida K, Yamanaka T, Sasaki T, Nakatsuka M, Mochizuki T, Kuroda J, Nakai S: Nd-doped phosphate glass laser systems for laser-fusion research. IEEE Journal of Quantum Electronics. 1981;17:1639–1649. DOI: 10.1109/JQE.1981.1071341

[19] Shimada Y, Nishimura H, Nakai M, Hashimoto K, Yamaura M, Tao Y, Shigemori K, Okuno T, Nishihara K, Kawamura T, Sunahara A, Nishikawa T, Sasaki A, Nagai K, Norimatsu T, Fujioka S, Uchida S, Miyanaga N, Izawa Y, Yamanaka C: Characterization of extreme ultraviolet emission from laser-produced spherical tin plasma generated with multiple laser beams. Applied Physics Letters. 2005;86:051501. DOI: 10.1063/1.1856697

[20] Yoshida K, Fujioka S, Higashiguchi T, Ugomori T, Tanaka N, Ohashi H, Kawasaki M, Suzuki Y, Suzuki C, Tomita K, Hirose R, Ejima T, Nishikino M, Sunahara A, Scally E, Li B, Yanagida T, Nishimura H, Azechi H, O'Sullivan G: Efficient extreme ultraviolet emission from one-dimensional spherical plasmas produced by multiple lasers. Applied Physics Express. 2014;7:086202. DOI: 10.7567/APEX.7.086202

[21] Masnavi M, Szilagyi J, Parchamy H, Richardson M. C: Laser-plasma source parameters for Kr, Gd, and Tb ions at 6.6 nm. Applied Physics Letters. 2013;102:164102. DOI: 10.1063/1.4802789

[22] Yoshida K, Fujioka S, Higashiguchi T, Ugomori T, Tanaka N, Kawasaki M, Suzuki Y, Suzuki C, Tomita K, Hirose R, Ejima T, Ohashi H, Nishikino M, Sunahara A, Li B,

Dunne P, O'Sullivan G, Yanagida T, Azechi H, Nishimura H: Density and x-ray emission profile relationships in highly ionized high-*Z* laser-produced plasmas. Applied Physics Letters. 2015;106:121109. DOI: 10.1063/1.4916395

[23] Ohashi H, Higashiguchi T, Li B, Suzuki Y, Kawasaki M, Kanehara T, Aida Y, Torii S, Makimura T, Jiang W, Dunne P, O'Sullivan G, Nakamura N: Tuning extreme ultraviolet emission for optimum coupling with multilayer mirrors for future lithography through control of ionic charge states. Journal of Applied Physics. 2014;115:033302. DOI: 10.1063/1.4862441; and references therein.

[24] Ohashi H, Higashiguchi T, Suzuki Y, Arai G, Otani Y, Yatagai T, Li B, Dunne P, O'Sullivan G, Jiang W, Endo A, Sakaue H. A, Kato D, Murakami I, Tamura N, Sudo S, Koike F, Suzuki C: Quasi-Moseley's law for strong narrow bandwidth soft x-ray sources containing higher charge-state ions. Applied Physics Letters. 2014;104:234107. DOI: 10.1063/1.4883475

[25] Colombant D, Tonon G. F: X-ray emission in laser-produced plasmas. Journal of Applied Physics.1973;44:3524-3537. DOI: 10.1063/1.1662796

[26] Higashiguchi T, Otsuka T, Yugami N, Jiang W, Endo A, Li B, Dunne P, O'Sullivan G: Feasibility study of broadband efficient "water window" source. Applied Physics Letters. 2012;100:014103. DOI: 10.1063/1.3673912; and references therein.